7756 *Biochemistry* **2009,** *48,* 7756–7763
DOI: 10.1021/bi900785x

BIOCHEMISTRY
including biophysical chemistry & molecular biology
Article

Smaller Discoidal High-Density Lipoprotein Particles Form Saddle Surfaces, but Not Planar Bilayers[†]

Masakazu Miyazaki, Minoru Nakano,* Masakazu Fukuda, and Tetsurou Handa

Graduate School of Pharmaceutical Sciences, Kyoto University, Sakyo-ku, Kyoto 606-8501, Japan

Received May 7, 2009; Revised Manuscript Received June 25, 2009

ABSTRACT: Discoidal high-density lipoprotein (HDL) particles are known to be fractionalized into several discrete populations in plasma and to differ in behavior according to size; however, their structural differences and the factors regulating their size are less understood. In this study, we prepared several reconstituted HDLs (rHDLs) for structural evaluation by gel filtration chromatography and fluorometric analyses. With initial ratios of phospholipid (PL) to apolipoprotein A-I (apoA-I) between 25:1 and 100:1, unsaturated PLs constructed rHDLs with diameters of 9.5−9.6, 8.8−9.0, and 7.8−7.9 nm. Conversely, saturated PLs formed only the largest type of rHDLs (9.5−9.9 nm). While the largest rHDL comprised 23% cholesterol (Chol), the smallest rHDL contained only 13% Chol, which approximates liquid-ordered phase composition. As the size of rHDLs decreased, both the lateral pressure in the lipid bilayer, as determined from the excimer fluorescence of dipyrenylphosphatidylcholine, and the degree of hydration of the membrane surface, which was examined using the mean fluorescence lifetime of dansyl phosphatidylethanolamine, decreased well below the values obtained for large unilamellar vesicles. These results demonstrated that smaller rHDLs form a saddle surface, distinct from the planar bilayer produced by the largest forms.

High-density lipoprotein (HDL)[1] transports excess cholesterol (Chol) in peripheral tissues to the liver for recycling and secretion into bile (*1*). This pathway, the reverse cholesterol transport (RCT), plays crucial roles in Chol homeostasis and protection against arteriosclerosis.

Apolipoprotein A-I (apoA-I) is a major protein component of HDL. HDL neogenesis arises during the interaction of apoA-I with transmembrane ATP-binding cassette transporter A1 (ABCA1) (*2*−*4*). Nascent HDLs have a discoidal form in which apoA-I molecules wrap around a lipid bilayer. Chol in this particle is converted to cholesteryl ester by lectin:cholesterol acyltransferase (LCAT), which changes discoidal HDLs into a spherical form with a greater Chol capacity (*5*, *6*).

The size distribution of discoidal HDLs shows several discrete populations in plasma (*7*). Similar discoidal particles can be reconstituted with phospholipids (PLs), Chol, and apoA-I in vitro (*8*−*10*). Physicochemical and biological studies with these reconstituted HDLs (rHDLs) have revealed that the functions of rHDL differ according to size. For example, LCAT's activation is directly related to rHDL size and apoA-I content. rHDL particles containing more than three apoA-I molecules have higher levels of LCAT activity than those containing two molecules, and among rHDLs containing two apoA-I molecules, the larger subclasses exhibit greater LCAT activity (*11*, *12*). In addition, cellular Chol efflux efficiency differs by the size of Chol acceptors (*13*); on a per particle basis, aqueous diffusion of cellular Chol to rHDL is more effective for larger particles. Therefore, it is important to elucidate the structural differences and factors regulating size among rHDLs of various dimensions.

Recently, Catte et al. have reported molecular dynamics simulations on smaller rHDLs containing 1-palmitoyl-2-oleoyl-*sn*-glycero-3-phosphocholine (POPC) with POPC:apoA-I molar ratios of 50:1 and 25:1 (*14*). They demonstrated that these particles no longer form planar bilayers but form a minimal surface instead. In negative-stain electron microscopy, smaller rHDLs appeared globular in shape with a lesser degree of rouleau formation (*11*, *14*), a morphology usually observed in larger particles.

To reveal the structure of smaller rHDLs, we prepared rHDLs with several lipid:apoA-I ratios and evaluated their size by gel filtration chromatography. In addition, the lipid packing state of rHDLs in both acyl chain and headgroup regions was analyzed using two fluorescence techniques (Figure 1): excimer formation of 1,2-bis(1-pyrenedecanoyl)-*sn*-glycero-3-phosphocholine (C_{10}dipyPC), which correlates to the lateral pressure in the acyl chain region (*15*, *16*), and the fluorescence lifetime of dansyl phosphatidylethanolamine, which is sensitive to headgroup packing (*17*). These approaches revealed that smaller rHDLs, which can be reconstituted only by unsaturated PLs, have a curved lipid bilayer and form a saddle surface.

[†]This study was supported by Grants-in-aid for Scientific Research from the Japanese Ministry of Education, Culture, Sports, Science and Technology (17390011, 20050017, and 20790032) and the program for the Promotion of Fundamental Studies in Health Science of the National Institute of Biomedical Innovation.

*To whom correspondence should be addressed. Telephone: +81-75-753-4565. Fax: +81-75-753-4601. E-mail: mnakano@pharm.kyoto-u.ac.jp.

[1]Abbreviations: apoA-I, apolipoprotein A-I; β-py-C_{10}-HPC, 1-hexadecanoyl-2-(1-pyrenedecanoyl)-*sn*-glycero-3-phosphocholine; C_{10}dipyPC, 1,2-bis(1-pyrenedecanoyl)-*sn*-glycero-3-phosphocholine; Chol, cholesterol; dansyl PE, egg yolk dansyl phosphatidylethanolamine; DMPC, 1,2-dimyristoyl-*sn*-glycero-3-phosphocholine; DOPC, 1,2-dioleoyl-*sn*-glycero-3-phosphocholine; DPPC, 1,2-dipalmitoyl-*sn*-glycero-3-phosphocholine; HDL, high-density lipoprotein; L_d phase, liquid-disordered phase; L_o phase, liquid-ordered phase; LUV, large unilamellar vesicle; PL, phospholipid; POPC, 1-palmitoyl-2-oleoyl-*sn*-glycero-3-phosphocholine; RCT, reverse cholesterol transport; rHDL, reconstituted HDL; Rho-DMPE, 1,2-dimyristoyl-*sn*-glycero-3-phosphoethanolamine-*N*-(Lissamine Rhodamine B Sulfonyl); Rho-DOPE, 1,2-dioleoyl-*sn*-glycero-3-phosphoethanolamine-*N*-(Lissamine Rhodamine B Sulfonyl); Rho-DPPE, 1,2-dipalmitoyl-*sn*-glycero-3-phosphoethanolamine-*N*-(Lissamine Rhodamine B Sulfonyl); Rho-PE, phosphoethanolamine-*N*-(Lissamine Rhodamine B Sulfonyl).

 Published on Web 07/18/2009

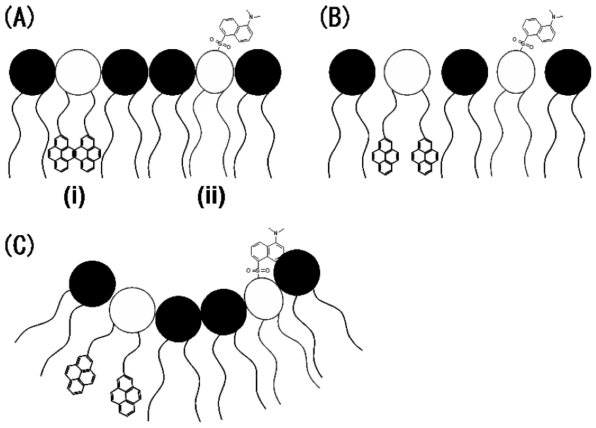

FIGURE 1: Schematic representation of fluorophores in lipid membranes with different packing states. (A) Planar lipid membrane. (B) Loosely packed membrane. (C) Negatively curved membrane. Excimer formation of C_{10}dipyPC (i) is correlated to the lateral pressure in the acyl chain region and is restrained in membranes B and C compared with membrane A. The fluorescence lifetime of dansyl PE (ii) is negatively correlated to the level of penetration of water into the headgroup region, and looser headgroup packing in membrane B, but not in membrane C, reduces the lifetime.

MATERIALS AND METHODS

Materials. 1-Palmitoyl-2-oleoyl-*sn*-glycero-3-phosphocholine (POPC), 1,2-dioleoyl-*sn*-glycero-3-phosphocholine (DOPC), 1,2-dimyristoyl-*sn*-glycero-3-phosphocholine (DMPC), 1,2-dipalmitoyl-*sn*-glycero-3-phosphocholine (DPPC), and Chol were purchased from Sigma-Aldrich (St. Louis, MO). 1,2-Dioleoyl-*sn*-glycero-3-phosphoethanolamine-*N*-(Lissamine Rhodamine B Sulfonyl) (Rho-DOPE), 1,2-dipalmitoyl-*sn*-glycero-3-phosphoethanolamine-*N*-(Lissamine Rhodamine B Sulfonyl) (Rho-DPPE), 1,2-dimyristoyl-*sn*-glycero-3-phosphoethanolamine-*N*-(Lissamine Rhodamine B Sulfonyl) (Rho-DMPE), and egg yolk dansyl phosphatidylethanolamine (dansyl PE) were from Avanti Polar Lipids (Alabaster, AL). 1-Hexadecanoyl-2-(1-pyrenedecanoyl)-*sn*-glycero-3-phosphocholine (β-py-C_{10}-HPC) and C_{10}dipyPC were from Invitrogen (Eugene, OR). ApoA-I was isolated from pig plasma using procedures described previously (*18*). Briefly, an HDL fraction with density in the range of 1.063−1.21 g/mL was isolated from pig plasma by density gradient ultracentrifugation. Subsequently, apoA-I was separated by the delipidation of HDL with a 3:2 mixture of ethanol and diethyl ether (v/v). The purity of apoA-I as determined by sodium dodecyl sulfate−polyacrylamide gel electrophoresis (SDS−PAGE) was greater than 95%. All other chemicals were of the highest reagent grade.

Sample Preparation. All rHDL particles were prepared by the sodium cholate dialysis method (*10*, *19*). The required amounts of a chloroform/methanol solution of PLs and Chol were mixed in a round-bottomed glass flask. For the samples labeled with the fluorescence probe, a chloroform/methanol solution of Rho-PE, β-py-C_{10}-HPC, C_{10}dipyPC, or dansyl PE was mixed with a lipid solution to yield 0.1 mol % total lipids. After the organic solvent was removed with an evaporator, the sample was dried overnight in vacuum. The dried mixture was vortexed in Tris-HCl buffer [10 mM Tris, 150 mM NaCl, 1 mM EDTA, and 0.01 g/mL NaN_3 (pH 7.4)]. Sodium deoxycholate (Cholate) was added at a PL:cholate ratio of 1:2, and then the mixture was vortexed and incubated until it was clear. ApoA-I was added to the lipid mixture at a PL:apoA-I molar ratio of 100:1, 50:1, or 25:1. For the preparation of Chol-containing rHDL, the POPC:apoA-I:Chol molar ratio was set to 25:1:2.5, 25:1:5, or 25:1:7.5. After overnight incubation, the mixture was dialyzed for 2 days against Tris-HCl buffer to remove the cholate. The incubation and dialysis were performed at different temperatures, depending on the lipids used, i.e., 4 °C for POPC and DOPC, 24 °C for DMPC, and 37 °C for DPPC. DPPC rHDL was reconstituted at 37 °C to avoid denaturation of apoA-I (*20*).

To prepare large unilamellar vesicles (LUVs), Tris-HCl buffer was added to the dried lipid mixture. The mixture was vortexed and frozen and thawed five times. Then, the dispersion was extruded through a polycarbonate filter with a pore size of 100 nm. The mean particle diameter of each dispersion was ca. 120 nm, as determined by dynamic light scattering measurements (Photal FPAR-1000, Otsuka Electronics Co., Osaka, Japan).

The concentrations of PLs and Chol were determined with enzyme assay kits from Wako (Osaka, Japan). Protein concentrations were determined by the method of Lowry et al. (*21*).

Gel Filtration Chromatography. The rHDL preparations were analyzed by gel filtration chromatography on a Superdex 200 column eluted with Tris-HCl buffer at a flow rate of 0.4 mL/min at room temperature. The rHDL samples were prepared with 0.1 mol % Rho-PE (Rho-DOPE for POPC and DOPC, Rho-DMPE for DMPC, and Rho-DPPE for DPPC rHDLs) and applied to the column. The elution profiles were monitored with a Hitachi (Tokyo, Japan) F-2500 fluorescence spectrometer, which enabled the detection of dual fluorescence simultaneously. Fluorescence from rhodamine was detected with excitation and emission wavelengths of 550 and 590 nm, respectively, and tryptophan fluorescence was detected at 285 and 350 nm at 25 °C. The PLs:apoA-I ratio in rHDLs was directly determined from the intensity of the elution peak by calibration with samples of known PL and apoA-I concentrations. The Stokes diameter of rHDL was determined by comparing K_{av} values given by the following equation with those of standard proteins with known diameters:

$$K_{av} = (V_e - V_o)/(V_t - V_o) \quad (1)$$

where V_o is the void volume, V_t is the total column volume, and V_e is the elution volume. The following standard proteins were used: thyroglobulin (Sigma), 17.0 nm; ferritin (Sigma), 12.2 nm; catalase (Wako), 10.4 nm; and BSA (Pierce, Rockford, IL), 7.1 nm. The standard curve provided the following relation:

$$\log(\text{diameter}) = -0.93K_{av} + 1.25 \quad (2)$$

Nondenaturing Gradient Gel Electrophoresis (*NDGGE*). To confirm the result given by gel filtration chromatography, we conducted NDGGE for rHDLs with POPC and DPPC. The rHDLs were prepared by sodium cholate dialysis at an initial molar ratio of PLs to apoA-I of 100:1 or 25:1. The preparations and molecular weight markers were fractionated on a 4 to 20% Tris-glycine gel (Invitrogen, Carlsbad, CA) and visualized with silver stain reagent. Molecular weight markers used were the same as those used for gel filtration chromatography.

Fluorescence Measurements. POPC rHDL samples containing either 0.1 mol % β-py-C_{10}-HPC or 0.1 mol % C_{10}dipyPC were prepared at a POPC:apoA-I ratio of 100:1 or 25:1 and applied to the column for gel filtration chromatography. Dual fluorescence from the eluate was detected at 378 nm (monomer) and 478 nm (excimer) with excitation at 345 nm and 25 °C on the Hitachi F-2500 instrument to determine the excimer to monomer fluorescence intensity ratio (I_e/I_m) of each subclass. The I_e/I_m value for POPC LUVs labeled with 0.1 mol % β-py-C_{10}-HPC or

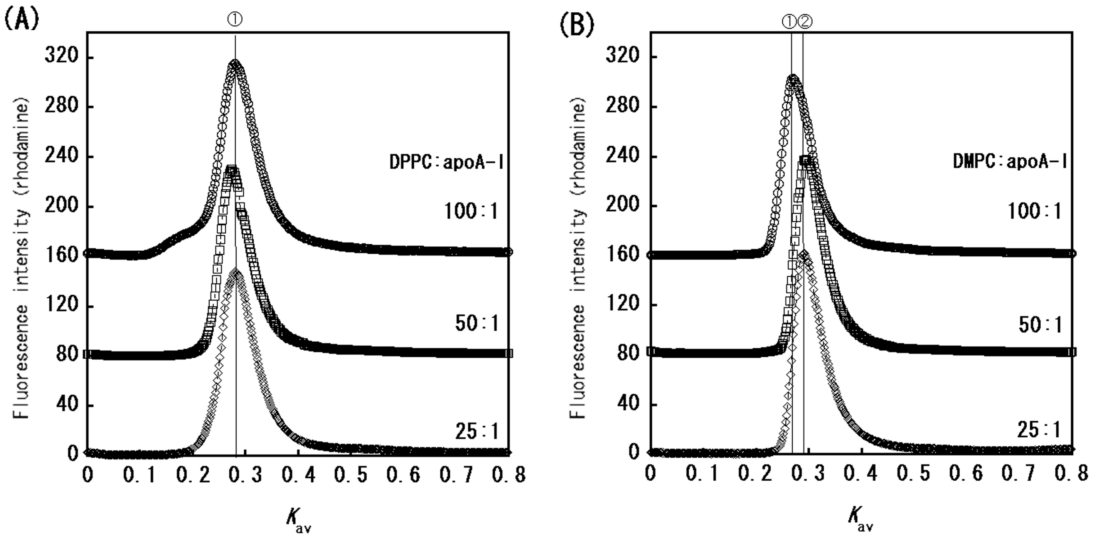

FIGURE 2: Gel filtration profiles of rHDLs with saturated PLs. rHDLs containing 0.1 mol % Rho-PE (Rho-DMPE for DMPC and Rho-DPPE for DPPC rHDLs) were prepared by sodium cholate dialysis and analyzed by gel filtration chromatography on a Superdex 200 column eluted with Tris-HCl buffer at a flow rate of 0.4 mL/min at room temperature: (A) initial DPPC:apoA-I ratios of 100:1 (○), 50:1 (□), and 25:1 (◇) and (B) initial DMPC:apoA-I ratios of 100:1 (○), 50:1 (□), and 25:1 (◇). The profiles were monitored using fluorescence from Rho-DPPE or Rho-DMPE.

0.1 mol % C_{10}dipyPC was measured by directly injecting the samples into a flow cell.

For fluorescence lifetime experiments, POPC rHDL samples containing 0.1 mol % dansyl PE were prepared at a POPC:apoA-I ratio of 100:1 or 25:1 and fractionated into each subclass by gel filtration. POPC LUVs labeled with 0.1 mol % dansyl PE were also prepared. The fluorescence lifetimes of dansyl PE in these samples were measured on a HORIBA (Kyoto, Japan) NAES-550 nanosecond fluorometer with a pulsed hydrogen lamp (full width at half-maximum of ~2 ns) and a thermostated cell holder. The samples were excited through a HOYA U350 filter, and their fluorescence was detected through a HOYA Y48 filter at 25 °C. The fluorescence decay curves were fitted as double exponentials with convolution of the intensity profile of pulsed excitation light by the HORIBA NAES-5X0 lifetime analysis program. Mean lifetime, $\langle\tau\rangle$, is defined by the following equation:

$$\langle\tau\rangle = \sum_{i=1}^{n} \alpha_i \tau_i^2 / \sum_{i=1}^{n} \alpha_i \tau_i \qquad (3)$$

where α_i and τ_i are the fractional amplitude and fluorescence lifetime, respectively, for the ith component.

RESULTS

Characterization of rHDLs with Saturated or Unsaturated PLs. To study the effects of acyl chain saturation and unsaturation on the size and composition of rHDLs, particles were prepared with POPC (C16:0,C18:1), DOPC (C18:1,C18:1), DMPC (C14:0,C14:0), or DPPC (C16:0,C16:0). The gel filtration chromatography profiles of lipids were monitored using the fluorescence of rhodamine. In the profiles for saturated PLs, the rHDL particle sizes calculated from the peaks were 9.5−9.9 nm (Figure 2 and Table 1). On the other hand, profiles for unsaturated PLs represented several discretely sized rHDL particle populations of 9.5−9.6, 8.8−9.0, and 7.8−7.9 nm (Figure 3 and Table 1). The size of the largest particle identified in the profiles of unsaturated PLs almost corresponded to that of saturated PLs. These results were also confirmed by nondenaturing gradient gel electrophoresis (Figure 4). Figure 5 shows the

Table 1: Stokes Diameters and PL:apoA-I Compositions of rHDLs

PL	peak number[a]	diameter (nm)[b,c]	PL:apoA-I[c,d] (mol/mol)
POPC	1	9.6 ± 0.1	78 ± 3.3
	2	9.0 ± 0.1	52 ± 1.3
	3	7.9 ± 0.1	25 ± 0.3
DOPC	1	9.5 ± 0.1	74 ± 0.6
	2	8.8 ± 0.1	52 ± 2.2
	3	7.8 ± 0.2	27 ± 1.2
DMPC	1	9.9 ± 0.1	95 ± 4.4
	2	9.5 ± 0.1	82 ± 6.9
DPPC	1	9.8 ± 0.1	92 ± 6.7

[a] From Figures 1 and 2. [b] Determined from gel filtration chromatography (see Materials and Methods). [c] The data represent means ± the standard deviations from at least four experiments. [d] Determined from rhodamine/tryptophan fluorescence.

superposition of rhodamine and tryptophan fluorescence profiles for a preparation with a DMPC:apoA-I ratio of 50:1 as a typical example. The K_{av} = 0.53 peak (corresponding to 5.7 nm), which was detected only by tryptophan fluorescence, is lipid-free apoA-I. On the other hand, the profiles for tryptophan and rhodamine overlapped at K_{av} = 0.29 (corresponding to 9.5 nm), which clearly denotes the presence of PL−apoA-I complexes. From these intensities, the PL:apoA-I ratio was calculated (Table 1). These results, especially for POPC rHDLs, were in good agreement with those obtained in the previous studies (*11*, *20*, *22*, *23*). The gel filtration profiles of the nonlabeled rHDLs (detected by tryptophan fluorescence) were the same as those of rhodamine-labeled rHDLs, suggesting that the labeling does not alter the characteristics of the particles (data not shown). Among the largest particles (POPC, 9.6 nm; DOPC, 9.5 nm; DMPC, 9.5 or 9.9 nm; and DPPC, 9.8 nm), the PL:apoA-I ratio was larger for saturated PLs than unsaturated PLs (Table 1). Assuming that the conformation of apoA-I in these particles is similar, this result implies that the saturated PLs in rHDL particles were tightly packed.

Effect of Cholesterol on POPC rHDLs. Chol is known to reduce membrane fluidity and increase the level of lipid packing in the liquid-disordered (L_d) phase (*24*). We prepared POPC rHDLs containing Chol to elucidate the effect of Chol on the

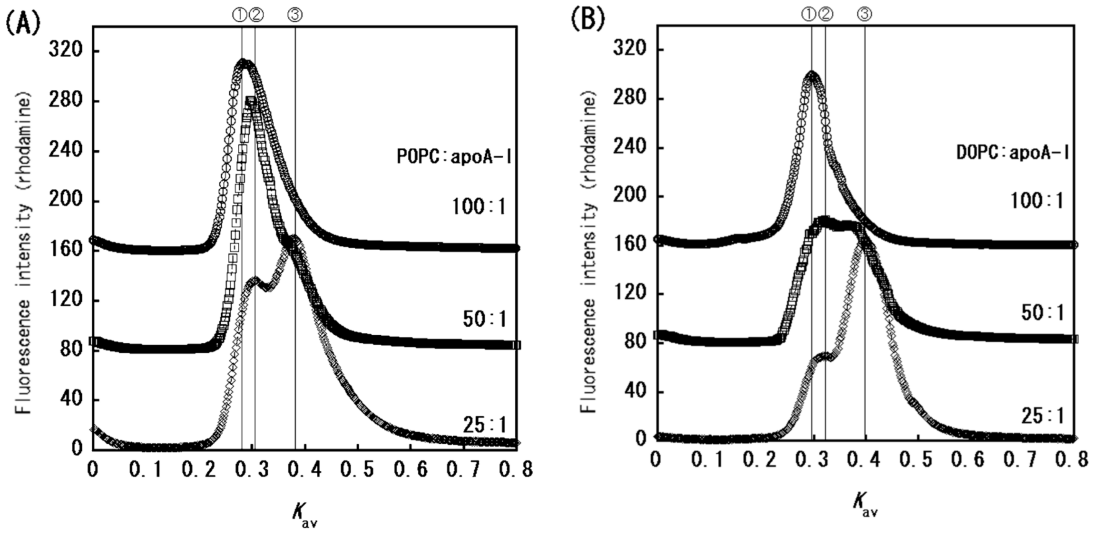

FIGURE 3: Gel filtration profiles of rHDLs with unsaturated PLs. Experiments were performed as described in the legend of Figure 2, except for the preparation of rHDL containing 0.1 mol % Rho-DOPE: (A) initial POPC:apoA-I ratios of 100:1 (○), 50:1 (□), and 25:1 (◇) and (B) initial DOPC:apoA-I ratios of 100:1 (○), 50:1 (□), and 25:1 (◇). The profiles were monitored using fluorescence from Rho-DOPE.

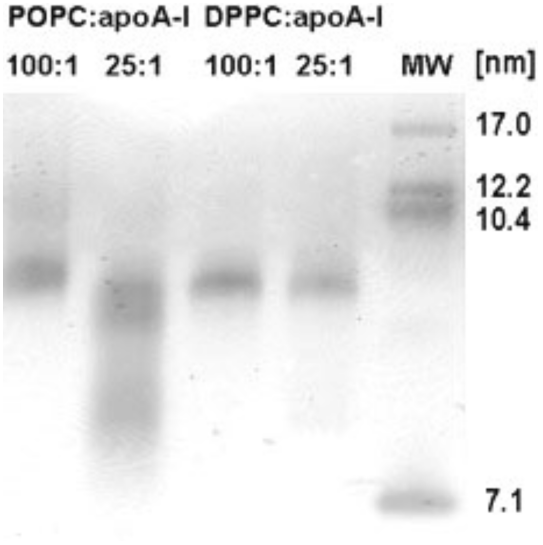

FIGURE 4: Nondenaturing gradient gel electrophoresis (NDGGE) analysis of rHDLs with POPC or DPPC. rHDLs were prepared by sodium cholate dialysis at an initial molar ratio of PLs to apoA-I of 100:1 or 25:1. The preparations and molecular weight markers were fractionated by 4 to 20% NDGGE and visualized with silver stain reagent. Molecular weight markers with known Stokes diameters are thyroglobulin (17.0 nm), ferritin (12.2 nm), catalase (10.4 nm), and BSA (7.1 nm).

formation of rHDLs. The initial POPC:apoA-I ratio was set to 25:1, and the Chol content was increased. With the increase in Chol content, the peak at 9.0 nm moved to 9.6 nm (Figure 6A), which corresponded to the size of the largest rHDL observed in Figure 3A. The peak at 7.9 nm was shifted slightly to 7.7 nm. To determine the Chol content of these particles, each rHDL fraction in gel filtration chromatography was separated and assayed for Chol and PL concentrations. As shown in Figure 6B, the Chol content of rHDL with a peak at 9.6 nm approximated that of the initial preparation. On the other hand, smaller rHDL (7.7 nm) included only ~13% Chol at most. Since POPC/Chol mixtures with a higher Chol content than this are known to form a liquid-ordered (L_o) phase (*25*, *26*), these results, together with the findings for rHDLs with saturated lipids, suggest that the smaller rHDL particles cannot be produced by closely packed and low-fluidity membranes.

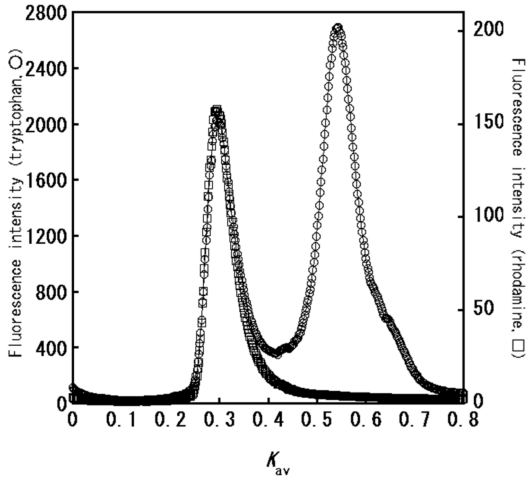

FIGURE 5: Superposition of lipid and protein elution profiles via gel filtration chromatography. rHDL with a DMPC:apoA-I ratio of 50:1 and 0.1 mol % Rho-DMPE was prepared. Elution profiles were simultaneously monitored for fluorescence from tryptophan (○) and Rho-DMPE (□).

Lateral Pressure in POPC rHDLs and LUV. To clarify the structural differences among rHDLs of various sizes, we evaluated the acyl chain's lateral pressure using the excimer fluorescence of C_{10}dipyPC. Intramolecular excimer is a transient complex between the ground state and excited state pyrene moieties, and an increase in the lateral pressure forces two pyrene moieties of C_{10}dipyPC to close with each other, which enhances the frequency of intramolecular excimer formation and increases the ratio of excimer (I_e) to monomer (I_m) fluorescence intensity (I_e/I_m) (*15*, *16*). POPC rHDL samples labeled with 0.1 mol % C_{10}dipyPC were eluted through the column, and the I_e and I_m of each subclass were monitored. For POPC LUVs, the I_e/I_m value was measured by directly injecting the samples into a flow cell. The results are shown in Figure 7. The I_e/I_m value of 9.6 nm rHDLs was slightly higher than that of LUVs, which implies that the lipid bilayer in 9.6 nm rHDL is more closely packed due to the presence of apoA-I belts. Interestingly, the I_e/I_m values for smaller (9.0 and 7.9 nm) rHDLs were markedly lower than the I_e/I_m value of 9.6 nm rHDL. These results suggest an increase

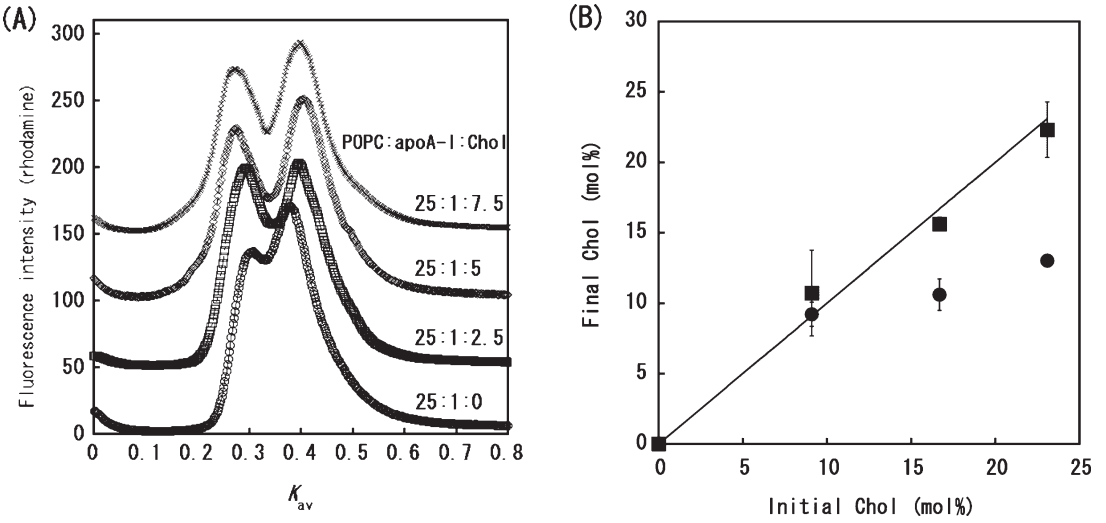

FIGURE 6: (A) Elution profiles of POPC/Chol rHDLs. Experiments were performed as described in the legend of Figure 2, except for the preparation of rHDL containing 0.1 mol % Rho-DOPE: initial POPC:apoA-I:Chol ratios of 25:1:0 (○), 25:1:2.5 (□), 25:1:5 (◇), and 25:1:7.5 (×). The profiles were monitored using fluorescence from Rho-DOPE. (B) Chol content of POPC/Chol rHDLs. Initial and final Chol denote the mole fractions of Chol against total lipids (PL + Chol) in the preparation and in rHDL fractionated by gel filtration [9.6 (□) and 7.7 nm (○)], respectively. The data represent means ± the standard deviation from three experiments. The solid line (slope = 1) represents the correspondence between the initial and final Chol contents.

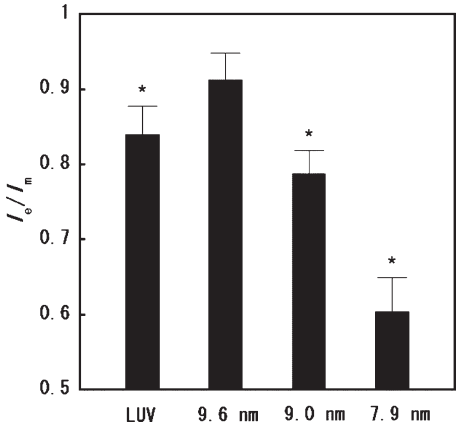

FIGURE 7: Excimer to monomer fluorescence intensity ratios (I_e/I_m) of C_{10}dipyPC in POPC rHDL particles (with diameters of 9.6, 9.0, and 7.9 nm) and LUV. The rHDL samples prepared at POPC:apoA-I ratios of 100:1 and 25:1 with 0.1 mol % C_{10}dipyPC were applied to the column for gel filtration chromatography, and dual fluorescence from the eluate was detected at 378 nm (I_m) and 478 nm (I_e) with excitation at 345 nm at 25 °C. Fluorescence from LUVs labeled with 0.1 mol % C_{10}dipyPC was measured by directly injecting the samples into a flow cell. The data represent means ± the standard deviation from four experiments. $P < 0.05$ (asterisk) by an unpaired *t*-test; significantly different from that of 9.6 nm rHDL.

in the average distance between the two pyrene moieties of C_{10}dipyPC in smaller rHDLs. We also prepared rHDLs and LUVs containing 0.1 mol % monofunctionalized β-py-C_{10}-HPC to confirm that the effect of the excimer intermolecular formation was negligible, and indeed, little excimer was detected ($I_e/I_m <$ 0.03).

Packing of PL Headgroups in POPC rHDLs and LUV. As described above, the extent of excimer formation of C_{10}dipyPC was reduced in smaller (9.0 and 7.9 nm) rHDLs, compared with that in 9.6 nm rHDL. Interpretation of this data raises two possibilities: either the pyrene moieties in smaller rHDLs are in a more loosely packed planar bilayer (Figure 1B), or they experience a negative curvature (Figure 1C). To distinguish between these possibilities, we performed fluorescence lifetime measurements with dansyl PE. The fluorescence lifetimes of fluorophores are sensitive to the surrounding environment and negatively correlate with the degree of hydration (*27*−*29*). Dansyl PE has a fluorophore at the phospholipid headgroup that enables evaluation of the membrane surface packing state (*17*). We prepared POPC rHDLs (fractionated into 9.6, 9.0, and 7.9 nm rHDLs) and POPC LUV with 0.1 mol % dansyl PE and determined their mean lifetime ($\langle\tau\rangle$). The results are shown in Figure 8. The $\langle\tau\rangle$ value of 9.6 nm rHDL was lower than that of LUV. This result could be ascribed to the presence of apoA-I belts: PL headgroups at the lipid−protein boundary of the bilayer edge are thought to be more exposed to water, leading to a decrease in the fluorescence lifetime. On the other hand, the $\langle\tau\rangle$ values increased as the size of the rHDL decreased. These results show that the membrane surface of smaller rHDLs is more closely packed, causing a decreased level of penetration of water into the membrane surface region. Taking into account the loose acyl chain packing, as suggested by the excimer fluorescence, we conclude that smaller rHDLs form a bilayer of negative curvature (Figure 1C). Particles of 7.9 nm, which exhibited the longest lifetime, would seem to have a more bent surface than a 9.0 nm rHDL.

DISCUSSION

Simulation-based studies have suggested several structural models of discoidal HDLs containing two apoA-I molecules, including the "picket-fence", "double-belt", and "helical-hairpin" models (*8*, *30*−*33*). Most of the experimental evidence supports the double-belt model, in which two apoA-I molecules surrounding a lipid bilayer are arranged in a continuous antiparallel amphipathic helix (*34*−*37*). In accordance with the length of apoA-I, 80 molecules of PL are surrounded by a single apoA-I in this model, which almost corresponds to the PL:apoA-I ratio for the largest particle with unsaturated PLs (Table 1).

The structure of smaller particles has been discussed previously. For example, in the "hinged-domain" model, one or more amphipathic α-helical segments of apoA-I undergo conformational changes to hinge off or on to the discoidal HDL edge (*38*). The "belt-buckle" model assumes that the N- and C-terminal

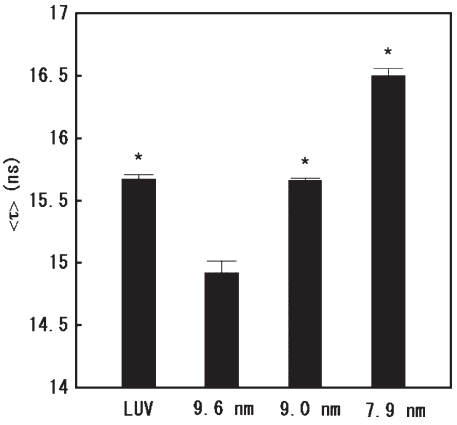

FIGURE 8: Mean fluorescence lifetime $\langle\tau\rangle$ of 0.1 mol % dansyl PE in POPC rHDL particles (with diameters of 9.6, 9.0, and 7.9 nm) and LUV. rHDLs (fractionated into each subclass by gel filtration) and LUVs labeled with 0.1 mol % dansyl PE were excited by pulsed excitation light passing through a HOYA U350 filter, and their fluorescence decay was detected with a HOYA Y48 filter at 25 °C. The data represent means ± the standard deviation from four experiments. $P < 0.05$ (asterisk) by an unpaired t-test; significantly different from that of 9.6 nm rHDL.

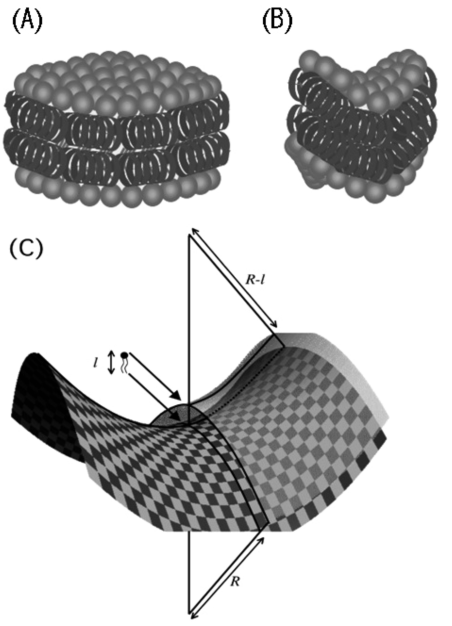

FIGURE 9: (A and B) Schematic representation of putative rHDL structures. Most of the discoidal HDL models suppose a planar bilayer (A), except for the twisted-belt model, which assumes that the bilayer forms a saddle surface (B). (C) Structure of minimal surface. Minimal surface (mosaic) with principal curvatures $\pm 1/R$ has a zero mean curvature and a negative Gaussian curvature ($-1/R^2$). At the lipid−water interface (gray), which lies apart from the minimal surface some distance l (lipid length), the mean curvature, $1/(R+l) - 1/(R-l)$, becomes a negative value.

ends of apoA-I in discoidal HDLs are folded back onto the belt (*22*, *39*), and the "solar-flares" model suggests that the loops at LCAT binding sites protrude from the edge of the discoidal HDL (*40*). All these models assume the discoidal HDL to be a planar lipid bilayer (Figure 9A). On the other hand, the "twisted-belt" model (*14*) is based on the crystal structure obtained from Δ1−43 apoA-I (*41*), which adopts a sharply curved horseshoe shape. Within the twisted apoA-I double belt, the lipid bilayer settles into a saddle-shaped, minimal surface (Figure 9B).

In this study, we prepared several rHDL particles with pig apoA-I. Pig apoA-I consists of 241 amino acids, which is two amino acids shorter than human apoA-I (*42*). The protein sequence, with a well-conserved secondary structural motif of amphipathic helices, is very homologous (79%) to human apoA-I. The rHDL particles characterized by gel filtration chromatography were almost identical to the ones prepared with human apoA-I (*11*, *20*, *22*, *23*). POPC rHDLs of 9.6 and 7.9 nm, and an "intermediate" particle with PL:apoA-I ratios of 80:1, 25:1, and 50:1, have been observed by Cavigiolio et al. (*11*). This trend was conserved for DOPC rHDL (Table 1). However, in the case of saturated PLs (DMPC and DPPC, whose gel−liquid crystalline phase transition temperatures are close to and higher than room temperature, respectively), smaller (<9.5 nm) rHDLs were not detected (Figure 2). In addition, 7.9 nm rHDL could not comprise PL/Chol lipid mixtures with an L_o phase. Saturated lipids and the L_o phase form planar rigid membranes with a high modulus of bending, due to a closely packed structure. Therefore, these results suggest that smaller rHDLs, unlike the 9.6 nm rHDL, do not adopt the planar structure but configure a surface of negative curvature. Differences in the spontaneous curvature of lipids (i.e., that saturated lipids have less negative curvature) may also account for the absence of smaller rHDLs of the saturated lipids.

Using larger DMPC rHDL particles (~11.7 nm), Massey et al. have found that Chol is a determinant of the structure of rHDLs (*43*). Our study suggests that smaller rHDLs cannot contain much Chol (Figure 6B). Therefore, Chol is an important factor affecting the structure of smaller rHDL particles as well. Chol is preferably distributed to a central lipid part of rHDLs away from the bilayer edge (*44*), which may partly contribute to the reduced Chol content in smaller rHDLs. However, the finding that the Chol capacity of smaller rHDL coincides with the Chol capacity of the L_d phase suggests that smaller rHDLs cannot be formed by the L_o phase, since the phase with the large bending modulus cannot adopt the curved surface.

A structure known as a minimal surface (saddle surface) exists in bicontinuous phases (*45*, *46*). In the bicontinuous cubic phases, the center of lipid bilayers constitutes the minimal surface, which has a zero mean curvature. However, because of a finite length of lipids that align normally to the minimal surface, the lipid−water interface holds a negative mean curvature (Figure 9C). Lipids on the minimal surface are thus constrained to occupy a smaller area at the lipid−water interface than the area at the bilayer center. Using the excimer fluorescence of C_{10}dipyPC and the fluorescence lifetime of 2-(9-anthroxy)stearic acid (2-AS), Kamo et al. demonstrated that the lamellar−bicontinuous cubic phase transition reduces the acyl chain's lateral pressure and increases the level of packing near the interface (*16*). Thus, these fluorescence techniques are sensitive to changes in the curvature of lipid membranes. In this study, we performed similar experiments to confirm the shape of smaller rHDLs, but we used dansyl PE instead of 2-AS because the former is more analogous to POPC. The fluorescence experiments revealed a reduction in the level of packing and an increase in the level of packing in the acyl chain and headgroup regions, respectively, as the size of rHDLs decreased. These results are similar to those observed in the lamellar−cubic phase transition (*16*) and suggest a minimal surface in rHDLs. Our results support the twist-belt model (*14*) since they cannot be explained by the other structural models that assume a planar lipid bilayer.

Catte et al. have proposed that 50:1 rHDL forms a minimal surface, whereas 25:1 rHDL has a lipid pocket capable of binding

a dynamic range of phospholipid molecules (*14*). However, taking the fluorescence lifetime values into consideration, if there were a flexible lipid pocket in the 25:1 particle, the lifetime of dansyl PE would have decreased because of an increase in the level of penetration of water. Thus, our results suggest that 25:1 rHDL forms a more bent saddle surface.

In summary, our experiments revealed that the lipid bilayer in smaller rHDL particles (50:1 and 25:1) forms a saddle surface (Figure 9B). These particles cannot be formed by low fluidity membranes (e.g., Chol-rich or saturated PLs). The differences in structure among rHDLs may affect their functions.

REFERENCES

1. Fielding, C. J., and Fielding, P. E. (1995) Molecular physiology of reverse cholesterol transport. *J. Lipid Res. 36*, 211–228.
2. Hassan, H. H., Bailey, D., Lee, D. Y., Iatan, I., Hafiane, A., Ruel, I., Krimbou, L., and Genest, J. (2008) Quantitative analysis of ABCA1-dependent compartmentalization and trafficking of apolipoprotein A-I: Implications for determining cellular kinetics of nascent high density lipoprotein biogenesis. *J. Biol. Chem. 283*, 11164–11175.
3. Denis, M., Landry, Y. D., and Zha, X. (2008) ATP-binding cassette A1-mediated lipidation of apolipoprotein A-I occurs at the plasma membrane and not in the endocytic compartments. *J. Biol. Chem. 283*, 16178–16186.
4. Vedhachalam, C., Duong, P. T., Nickel, M., Nguyen, D., Dhanasekaran, P., Saito, H., Rothblat, G. H., Lund-Katz, S., and Phillips, M. C. (2007) Mechanism of ATP-binding cassette transporter A1-mediated cellular lipid efflux to apolipoprotein A-I and formation of high density lipoprotein particles. *J. Biol. Chem. 282*, 25123–25130.
5. Curtiss, L. K., Valenta, D. T., Hime, N. J., and Rye, K. A. (2006) What is so special about apolipoprotein AI in reverse cholesterol transport?. *Arterioscler. Thromb. Vasc. Biol. 26*, 12–19.
6. Zannis, V. I., Chroni, A., and Krieger, M. (2006) Role of apoA-I, ABCA1, LCAT, and SR-BI in the biogenesis of HDL. *J. Mol. Med. 84*, 276–294.
7. Nichols, A. V., Gong, E. L., Blanche, P. J., Forte, T. M., and Anderson, D. M. (1976) Effects of guanidine hydrochloride on human plasma high density lipoproteins. *Biochim. Biophys. Acta 446*, 226–239.
8. Silva, R. A., Hilliard, G. M., Li, L., Segrest, J. P., and Davidson, W. S. (2005) A mass spectrometric determination of the conformation of dimeric apolipoprotein A-I in discoidal high density lipoproteins. *Biochemistry 44*, 8600–8607.
9. Nichols, A. V., Gong, E. L., Blanche, P. J., and Forte, T. M. (1983) Characterization of discoidal complexes of phosphatidylcholine, apolipoprotein A-I and cholesterol by gradient gel electrophoresis. *Biochim. Biophys. Acta 750*, 353–364.
10. Matz, C. E., and Jonas, A. (1982) Micellar complexes of human apolipoprotein A-I with phosphatidylcholines and cholesterol prepared from cholate-lipid dispersions. *J. Biol. Chem. 257*, 4535–4540.
11. Cavigiolio, G., Shao, B., Geier, E. G., Ren, G., Heinecke, J. W., and Oda, M. N. (2008) The interplay between size, morphology, stability, and functionality of high-density lipoprotein subclasses. *Biochemistry 47*, 4770–4779.
12. Meng, Q. H., Calabresi, L., Fruchart, J. C., and Marcel, Y. L. (1993) Apolipoprotein A-I domains involved in the activation of lecithin: cholesterol acyltransferase. Importance of the central domain. *J. Biol. Chem. 268*, 16966–16973.
13. Davidson, W. S., Rodrigueza, W. V., Lund-Katz, S., Johnson, W. J., Rothblat, G. H., and Phillips, M. C. (1995) Effects of acceptor particle size on the efflux of cellular free cholesterol. *J. Biol. Chem. 270*, 17106–17113.
14. Catte, A., Patterson, J. C., Jones, M. K., Jerome, W. G., Bashtovyy, D., Su, Z., Gu, F., Chen, J., Aliste, M. P., Harvey, S. C., Li, L., Weinstein, G., and Segrest, J. P. (2006) Novel changes in discoidal high density lipoprotein morphology: A molecular dynamics study. *Biophys. J. 90*, 4345–4360.
15. Templer, R. H., Castle, S. J., Curran, A. R., Rumbles, G., and Klug, D. R. (1998) Sensing isothermal changes in the lateral pressure in model membranes using di-pyrenyl phosphatidylcholine. *Faraday Discuss. 111*, 41–53 (discussion, 69−78).
16. Kamo, T., Nakano, M., Kuroda, Y., and Handa, T. (2006) Effects of an amphipathic α-helical peptide on lateral pressure and water penetration in phosphatidylcholine and monoolein mixed membranes. *J. Phys. Chem. B 110*, 24987–24992.
17. Nyholm, T., Nylund, M., Söderholm, A., and Slotte, J. P. (2003) Properties of palmitoyl phosphatidylcholine, sphingomyelin, and dihydrosphingomyelin bilayer membranes as reported by different fluorescent reporter molecules. *Biophys. J. 84*, 987–997.
18. Handa, T., Saito, H., Tanaka, I., Kakee, A., Tanaka, K., and Miyajima, K. (1992) Lateral interactions of pig apolipoprotein A-1 with egg yolk phosphatidylcholine and with cholesterol in mixed monolayers at the triolein-saline interface. *Biochemistry 31*, 1415–1420.
19. Jonas, A. (1986) Reconstitution of high-density lipoproteins. *Methods Enzymol. 128*, 553–582.
20. Davidson, W. S., Gillotte, K. L., Lund-Katz, S., Johnson, W. J., Rothblat, G. H., and Phillips, M. C. (1994) The effect of high density lipoprotein phospholipid acyl chain composition on the efflux of cellular free cholesterol. *J. Biol. Chem. 270*, 5882–5890.
21. Lowry, O. H., Rosebrough, N. J., Farr, A. L., and Randall, R. J. (1951) Protein measurement with the Folin phenol reagent. *J. Biol. Chem. 193*, 265–275.
22. Bhat, S., Sorci-Thomas, M. G., Tuladhar, R., Samuel, M. P., and Thomas, M. J. (2007) Conformational adaptation of apolipoprotein A-I to discretely sized phospholipid complexes. *Biochemistry 46*, 7811–7821.
23. Jonas, A., Wald, J. H., Toohill, K. L., Krul, E. S., and Kézdy, K. E. (1990) Apolipoprotein A-I structure and lipid properties in homogeneous, reconstituted spherical and discoidal high density lipoproteins. *J. Biol. Chem. 265*, 22123–22129.
24. Shinozawa, S., Araki, Y., Utsumi, K., and Oda, T. (1979) Stabilizing effects of cholesterol on changes in membrane permeability and potential induced in red blood cells by lysolecithin. *Physiol. Chem. Phys. 11*, 161–167.
25. de Almeida, R. F., Fedorov, A., and Prieto, M. (2003) Sphingomyelin/phosphatidylcholine/cholesterol phase diagram: Boundaries and composition of lipid rafts. *Biophys. J. 85*, 2406–2416.
26. Rappolt, M., Vidal, M. F., Kriechbaum, M., Steinhart, M., Amenitsch, H., Bernstorff, S., and Laggner, P. (2002) Structural, dynamic and mechanical properties of POPC at low cholesterol concentration studied in pressure/temperature space. *Eur. Biophys. J. 31*, 575–585.
27. Straume, M., and Litman, B. J. (1987) Equilibrium and dynamic structure of large, unilamellar, unsaturated acyl chain phosphatidylcholine vesicles. Higher order analysis of 1,6-diphenyl-1,3,5-hexatriene and 1-[4-(trimethylammonio)phenyl]-6-phenyl-1,3,5-hexatriene anisotropy decay. *Biochemistry 26*, 5113–5120.
28. Straume, M., and Litman, B. J. (1987) Influence of cholesterol on equilibrium and dynamic bilayer structure of unsaturated acyl chain phosphatidylcholine vesicles as determined from higher order analysis of fluorescence anisotropy decay. *Biochemistry 26*, 5121–5126.
29. Fiorini, R. M., Valentino, M., Glaser, M., Gratton, E., and Curatola, G. (1988) Fluorescence lifetime distributions of 1,6-diphenyl-1,3,5-hexatriene reveal the effect of cholesterol on the microheterogeneity of erythrocyte membrane. *Biochim. Biophys. Acta 939*, 485–492.
30. Tall, A. R., Small, D. M., Deckelbaum, R. J., and Shipley, G. G. (1977) Structure and thermodynamic properties of high density lipoprotein recombinants. *J. Biol. Chem. 252*, 4701–4711.
31. Davidson, W. S., and Silva, R. A. (2005) Apolipoprotein structural organization in high density lipoproteins: Belts, bundles, hinges and hairpins. *Curr. Opin. Lipidol. 16*, 295–300.
32. Koppaka, V. (2001) Structural studies of discoidal lipoprotein A-I. *Cell. Mol. Life Sci. 58*, 885–893.
33. Gursky, O. (2005) Apolipoprotein structure and dynamics. *Curr. Opin. Lipidol. 16*, 287–294.
34. Li, H., Lyles, D. S., Thomas, M. J., Pan, W., and Sorci-Thomas, M. G. (2000) Structural determination of lipid-bound ApoA-I using fluorescence resonance energy transfer. *J. Biol. Chem. 275*, 37048–37054.
35. Panagotopulos, S. E., Horace, E. M., Maiorano, J. N., and Davidson, W. S. (2001) Apolipoprotein A-I adopts a belt-like orientation in reconstituted high density lipoproteins. *J. Biol. Chem. 276*, 42965–42970.
36. Gorshkova, I. N., Liu, T., Kan, H. Y., Chroni, A., Zannis, V. I., and Atkinson, D. (2006) Structure and stability of apolipoprotein a-I in solution and in discoidal high-density lipoprotein probed by double charge ablation and deletion mutation. *Biochemistry 45*, 1242–1254.
37. Shih, A. Y., Arkhipov, A., Freddolino, P. L., Sligar, S. G., and Schulten, K. (2007) Assembly of lipids and proteins into lipoprotein particles. *J. Phys. Chem. B 111*, 11095–11104.
38. Li, L., Chen, J., Mishra, V. K., Kurtz, J. A., Cao, D., Klon, A. E., Harvey, S. C., Anantharamaiah, G. M., and Segrest, J. P. (2004) Double belt structure of discoidal high density lipoproteins: Molecular basis for size heterogeneity. *J. Mol. Biol. 343*, 1293–1311.
39. Bhat, S., Sorci-Thomas, M. G., Alexander, E. T., Samuel, M. P., and Thomas, M. J. (2005) Intermolecular contact between globular

N-terminal fold and C-terminal domain of ApoA-I stabilizes its lipid-bound conformation: Studies employing chemical cross-linking and mass spectrometry. *J. Biol. Chem. 280*, 33015–33025.
40. Wu, Z., Wagner, M. A., Zheng, L., Parks, J. S.III, Shy, J. M., Smith, J. D., Gogonea, V., and Hazen, S. L. (2007) The refined structure of nascent HDL reveals a key functional domain for particle maturation and dysfunction. *Nat. Struct. Mol. Biol. 14*, 861–868.
41. Borhani, D. W., Rogers, D. P., Engler, J. A., and Brouillette, C. G. (1997) Crystal structure of truncated human apolipoprotein A-I suggests a lipid-bound conformation. *Proc. Natl. Acad. Sci. U.S.A. 94*, 12291–12296.
42. Birchbauer, A., Knipping, G., Juritsch, B., Aschauer, H., and Zechner, R. (1993) Characterization of the apolipoprotein AI and CIII genes in the domestic pig. *Genomics 15*, 643–652.
43. Massey, J. B., and Pownall, H. J. (2008) Cholesterol is a determinant of the structures of discoidal high density lipoproteins formed by the solubilization of phospholipid membranes by apolipoprotein A-I. *Biochim. Biophys. Acta 1781*, 245–253.
44. Dergunov, A. D., Dobretsov, G. E., Visvikis, S., and Siest, G. (2001) Protein-lipid interactions in reconstituted high density lipoproteins: Apolipoprotein and cholesterol influence. *Chem. Phys. Lipids 113*, 67–82.
45. Lindblom, G., and Rilfors, L. (1989) Cubic phases and isotropic structures formed by membrane lipids-possible biological relevance. *Biochim. Biophys. Acta 988*, 221–256.
46. Seddon, J. M. (1990) Structure of the inverted hexagonal (HII) phase, and non-lamellar phase transitions of lipids. *Biochim. Biophys. Acta 1031*, 1–69.